

Article

The Effects of Benzene on the Structure and Properties of Triethylamine Hydrochloride/Chloroaluminate

Guocai Tian * , Huanhuan Du and Qingxiang Yuan

State Key Laboratory of Complex Non-Ferrous Metal Resource Clean Utilization, Faculty of Metallurgical and Energy Engineering, Kunming University of Science and Technology, Kunming 650093, China; yunduoxiaoshan@163.com (H.D.); yuanqx01@163.com (Q.Y.)

* Correspondence: tiangc@kust.edu.cn; Tel.: +86-871-6519-8154

Abstract: The effects of benzene (C_6H_6) on the radial distribution function, coordination number, spatial distribution function, physical and chemical properties such as density, viscosity, conductivity and transport properties of triethylamine hydrochloride /chloroaluminate ($[Et_3NH] Cl / AlCl_3$) ionic liquid were studied by first principle and molecular dynamics simulation. The stable geometry and electronic properties of benzene and ionic liquids, as well as their optimized adsorption on Cu (111) surface were obtained. The density, viscosity and conductivity obtained agreed well with the experimental values. It is found that the adsorption of cations, anions and benzene on Cu (111) surface is physical adsorption, and the adsorption capacity is $[Et_3NH] > C_6H_6 > Al_2Cl_7^-$. With the increase of benzene concentration, the density of the system decreases gradually, the interaction between cations and anions gradually weakens, resulting in the decrease of viscosity, the enhancement of diffusion and the increase of conductivity. Since the diffusion and adsorption capacity of benzene are greater than that of electroactive ion of $Al_2Cl_7^-$, benzene would be easier to adsorb on the protruding part of the electrode surface, so as to reduce the effective surface area of the cathode, slow down the reduction speed of $Al_2Cl_7^-$ on the cathode surface and increase the over-potential, so the grain refined deposition layers can be obtained in electrodeposition.

Keywords: ionic liquids; triethylamine hydrochloride/chloroaluminate; benzene; first principles; molecular dynamics; microstructure; adsorption; diffusion



Citation: Tian, G.; Du, H.; Yuan, Q. The Effects of Benzene on the Structure and Properties of Triethylamine Hydrochloride/Chloroaluminate. *Crystals* **2021**, *11*, 1532. <https://doi.org/10.3390/cryst11121532>

Academic Editor: Shujun Zhang

Received: 12 November 2021

Accepted: 7 December 2021

Published: 8 December 2021

Publisher's Note: MDPI stays neutral with regard to jurisdictional claims in published maps and institutional affiliations.



Copyright: © 2021 by the authors. Licensee MDPI, Basel, Switzerland. This article is an open access article distributed under the terms and conditions of the Creative Commons Attribution (CC BY) license (<https://creativecommons.org/licenses/by/4.0/>).

1. Introduction

Ionic liquid, also known as room temperature molten salts, is an ionic system in the liquid state at or near room temperature. It is usually composed of organic cations and inorganic or organic anions [1,2]. It has the characteristics of a good thermal stability, wide liquid temperature range, wide electrochemical window, good conductivity, non-volatile and variable property combination. It has been extensively used in many fields such as metal electrodeposition, electrochemistry, battery and catalysis [3–8]. In particular, it has aroused great interest in electrodeposition and electrolysis of active metals [2,3,6,8].

Aluminum is the foundation and strategic material for national economy and national defense construction, strategic emerging industries, aerospace, etc. At present, Hall–Héroult process, namely cryolite alumina molten salt electrolysis method, is usually used for industrial production of aluminum [9]. It has some disadvantages, such as high-energy consumption, large CO_2 emission, and serious equipment corrosion and so on. Therefore, the research and development of new aluminum electrolysis technology with high efficiency, energy conservation and environmental protection are of great significance. The emergence of room temperature molten salt ionic liquid provides a possibility for the development of low temperature electrolytic aluminum technology [10–20]. In 1992, Carlin et al. [10] electrolysis metal aluminum at room temperature with chloride-1-ethyl-3-methylimidazole/chloroaluminate ($[Emim]Cl / AlCl_3$) ionic liquid, which attracted great interest of researchers. In recent years, significant progress has been made in re-

lated research [11–20]. Generally, aluminum electrodeposition and electrolytic refining in ionic liquids mostly use imidazole chloride and chloroaluminate system, which are sensitive to water and air and has relatively high cost. Therefore, it is necessary to find an ionic liquid system with excellent stability and low cost. Quaternary ammonium ionic liquids are favored by researchers because of their advantages of low cost, high conductivity and superior quality of metal deposition layer [21–27]. Triethylamine hydrochloride/chloroaluminate ($[\text{Et}_3\text{NH}]\text{Cl}/\text{AlCl}_3$) is one of the most-used systems. The values of conductivity of $[\text{Et}_3\text{NH}]\text{Cl}/\text{AlCl}_3$ with an AlCl_3 mole fraction of 0.667 is comparable with the corresponding data of 1-butyl-3-methylimidazolium chloride ($[\text{Bmim}]\text{Cl}$) system at the same temperature and the same mole fraction, even though the viscosity value of $[\text{Et}_3\text{NH}]\text{Cl}/\text{AlCl}_3$ system is a little higher. From this comparison, it is believed that $[\text{Et}_3\text{NH}]\text{Cl}/\text{AlCl}_3$ electrolyte is a good candidate to substitute $[\text{Bmim}]\text{Cl}/\text{AlCl}_3$ system in view of easy availability and low price. Recent years, $[\text{Et}_3\text{NH}]\text{Cl}/\text{AlCl}_3$ has been widely and successfully used in electrochemistry, cell, and catalysis fields [21–27].

It is found that electrodeposited aluminum or electrolytic refined aluminum in ionic liquid can significantly reduce the temperature and DC unit consumption, and there are no CO_2 and other gas emissions, which can effectively reduce energy consumption and environmental pollution, and meet the requirements of green development. However, there are still some problems with this method, such as poor quality of deposition layer, serious dendrite phenomenon and low current efficiency, which need to be further solved [8,19]. The addition of inorganic or organic additives is one of the most used methods to solve these problems. In recent years, the effect of additives on the quality of aluminum deposit in imidazole-type ionic liquids has been studied, and some progress has been achieved [13]. Benzene (C_6H_6), as a cyclic aromatic compound with delocalized π electrons, has been widely used as an additive in ionic liquid electrodeposition of aluminum [28–30]. It is noted that a smooth and bright aluminum deposit can be obtained after the addition of benzene. Xia et al. studied the effect of C_6H_6 on the properties of triethylamine hydrochloride ionic liquid $[\text{Et}_3\text{NH}]\text{Cl}/\text{AlCl}_3$ electrolyte system [30]. It is noted that the addition of C_6H_6 can reduce the viscosity and increase the conductivity of the system. However, as a new green solvent and electrolyte system, the related research of ionic liquid is not in-depth. How to select efficient additives, the effects of additives on the microstructure, physical and chemical properties of the system, and the mechanism of aluminum deposition are still not clear. In recent years, first principles and molecular dynamics simulation have been widely used to study the microstructure, physical and chemical properties and kinetic characteristics of a condensed phase system, and achieved certain results [31–36], which provides a good idea for the study of the action mechanism of additives.

In this paper, the low-cost and widely used triethylamine hydrochloride ionic liquids $[\text{Et}_3\text{NH}]\text{Cl}/\text{AlCl}_3$ [30] is taken as the research object. We mainly focus on the effect of benzene addition on the micro-structure, physical and chemical properties, diffusion as well as the adsorption behavior molecules or ions in $[\text{Et}_3\text{NH}]\text{Cl}/\text{AlCl}_3$ ionic liquids system through ab initio calculation and simulation. The first principle calculation and molecular dynamics are combined to systematically study the adsorption of benzene C_6H_6 , cation and anion of $[\text{Et}_3\text{NH}]\text{Cl}/\text{AlCl}_3$ on the surface of Cu (111), the effect of benzene on the formation of ions, interaction, physical and chemical properties, diffusion and transport characteristics of particles in the $[\text{Et}_3\text{NH}]\text{Cl}/\text{AlCl}_3$ system. The research work will provide the theoretical guidance and support for the application and research of this kind of ionic liquids.

2. Materials and Methods

The geometry optimization and vibration frequency analysis of benzene C_6H_6 and $[\text{Et}_3\text{NH}]\text{Cl}/\text{AlCl}_3$ ionic liquids were performed at the 6-311++G(d,p) level by using the B3LYP method of density functional theory in Gaussian 09 [37]. Firstly, the geometric structures of anions, cations, ion pairs and benzene molecules are optimized with full optimization. Then, vibration frequency analysis was implemented to confirm a stable geometry structure, which is no negative frequency. After that the stable geometry was

used to calculate the relevant properties of target molecules or ions, such as the highest occupied molecular orbitals (HOMO), the lowest unoccupied molecular orbitals (LUMO), and the electrostatic potential.

The effects of benzene on the microstructure, diffusion, and the physical and chemical properties of $[\text{Et}_3\text{NH}]\text{Cl}/\text{AlCl}_3$ were revealed by a scalable parallel molecular dynamics package of MDynaMix 4.3 [38]. Optimized geometry of $[\text{Et}_3\text{NH}]^+$, Cl^- , AlCl_3 and C_6H_6 molecules are shown in Figure 1. AMBER force fields was applied, in which the force field parameters of $[\text{Et}_3\text{NH}]^+$ developed by Wang et al. [39] were used. The force field parameters of C_6H_6 were developed by Kim et al. [40], and the force field parameters of Cl^- and AlCl_3 were developed by Andrade et al. [41]. The atomic charge of the cation $[\text{Et}_3\text{NH}]^+$ is obtained by the restrained electrostatic potential (RESP) approach [42]. The dipole moment of the $[\text{Et}_3\text{NH}]^+$ obtained by the RESP method is 0.3685 D, which is in good agreement with the 0.3662 D obtained by the first principle calculation, indicating that the calculated RESP charge in the present manuscript is accurate. Various $[\text{Et}_3\text{NH}]^+$, Cl^- , AlCl_3 and C_6H_6 molecules or ions are randomly placed in the simulation box with their initial configuration in Figure 1. It is well-known that the predominant presence of anions can be expressed as AlCl_4^- and Al_2Cl_7^- , respectively. With the increase of mole fraction of AlCl_3 , the molar concentration of Al_2Cl_7^- increases, when the mole fraction of AlCl_3 is 0.667 in $[\text{Et}_3\text{NH}]\text{Cl}/\text{AlCl}_3$, the predominant presence of anions is Al_2Cl_7^- . Therefore, the mole ration of 1:2 for $[\text{Et}_3\text{NH}]\text{Cl}$ and AlCl_3 are used for $[\text{Et}_3\text{NH}]\text{Cl}/\text{AlCl}_3$ in present work. In order to compare with the experimental results in ref. [30], the mole fraction of benzene of 0, 0.19, 0.32, 0.41, 0.48, 0.53 on the structure and properties of $[\text{Et}_3\text{NH}]\text{Cl}/\text{AlCl}_3$ systems were studied. The particle number in the simulation system and the size of the simulation box in equilibrium are shown in Table 1. Three-dimensional periodic boundary conditions were implemented. The initial velocity is randomly generated from the Maxwell distribution according to the simulated temperature of 298.15K. The electrostatic interaction is treated by the Ewald summation technique. The motion equation is solved by Tuckerman-Berne double time-step algorithm. The long-time and short-time steps are 2 fs and 0.2 fs, respectively. Firstly, systems were equilibrated in NPT ensemble with 400 ps to reach the equilibrium. The simulated density is in good agreement with their experimental value. Then, the final equilibration configurations of the NPT ensemble were used as the initial configurations to perform the simulation in NVT ensemble for 2 ns, and the trajectory was saved every 10 steps for subsequent analysis and physical quantity calculation.

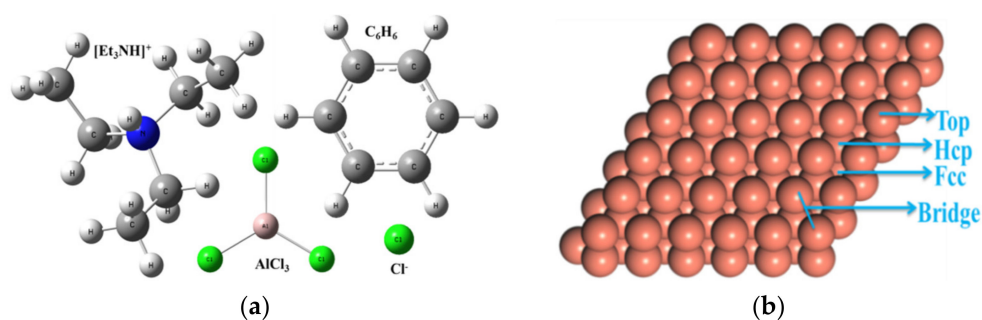


Figure 1. The stable geometry of molecules or ions in molecular dynamics simulation (a) and the schematic diagram of different adsorption sites on Cu(111) surface (b).

Table 1. Particle numbers, equilibrium box sizes, simulated density and experimental density of [Et₃NH]Cl/AlCl₃ with different mole fractions of C₆H₆.

Mole Fraction of C ₆ H ₆	[Et ₃ NH]Cl	AlCl ₃	C ₆ H ₆	Equilibrium Sizes of Simulation Box (nm ³)	$\rho_{sim}/g \cdot cm^{-3}$	$\rho_{exp}/g \cdot cm^{-3}$ [30]
0	128	256	0	4.047 × 4.047 × 4.047	1.297	1.312
0.19	128	256	88	4.301 × 4.301 × 4.301	1.223	1.248
0.32	128	256	177	4.506 × 4.506 × 4.506	1.190	1.201
0.41	128	256	265	4.713 × 4.713 × 4.713	1.149	1.169
0.48	128	256	353	4.916 × 4.916 × 4.916	1.109	1.128
0.53	128	256	441	5.082 × 5.082 × 5.082	1.091	1.095

Since copper is commonly used as a cathode for the electrodeposition of aluminum in ionic liquids, the adsorption of benzene, anion and cation on the copper surface Cu (111) was studied in the present work by Vienna ab initio simulation package (VASP) code of VASP 5.4.1 [43,44]. The exchange correlation functional of Perdew-Burke-Ernzerhof (PBE) [45] of Generalized Gradient Approximation (GGA) in Density Functional Theory (DFT) was utilized. The D3-BJ method proposed by Grimme [46] was used to consider van der Waals interaction. The convergence criterion of the force is 0.01 eV/Å, the energy convergence standard is 10⁻⁴ eV. The cutoff energy is 400 eV, and the Methfessel Paxton broadening is 0.2 eV. The lattice constant of the optimized Cu cell is 3.615 Å, which is in good agreement with previous experimental and theoretical results [47,48].

The Cu(111) surface was modeled using a four-layered model p(6 × 6) super cell (as showed in Figure 1). As showed by Avalentín, four layers model can meet the convergence requirements for molecules or ions adsorption on Cu(111) [49]. The supercell size is 16.66 × 16.66 × 30.40 Å³ and the surfaces were separated by a vacuum layer of 22.91 Å. The Brillouin zone is sampled by 3 × 3 × 1 k-points using the Monkhorst-Pack scheme [50]. We considered the adsorption of the molecules or ions at four different positions on Cu (111) surface as showed in Figure 1. It is found that the target system is more inclined to be adsorbed at the Hcp site of Cu (111). Therefore, we will just focus on the adsorption of molecules or ions at the Hcp site of Cu (111). The adsorption energy is calculated by $E_{ads} = E_{(mol/surf)} - (E_{surf} + E_{mol})$, where $E_{(mol/surf)}$ is the total energy of stable adsorption structure of Cu (111) surface and the adsorbed molecules or ions. E_{surf} is the energy of Cu (111) surface, where E_{mol} is the energy of molecules or ions. Atomic charges of the system were analyzed by Bader method [51], and the differential charge density diagrams were obtained by VESTA software [52]. Frontier orbitals and electrostatic potential diagram were obtained by Multiwfn [53] and VMD [54] software according to the results of quantum chemistry calculation.

3. Results and Discussion

3.1. Effect of Additives on Microstructure and Physicochemical Properties of the System

3.1.1. Density

The densities of [Et₃NH]Cl/AlCl₃ and C₆H₆ at 298.15 K and 0.1 MPa obtained from molecular dynamics simulation are 1.297 g/cm³ and 0.8511 g/cm³ respectively, which are in good agreement with the experimental values of 1.312 g/cm³ [30] and 0.874 g/cm³ [30]. It is shown that the applied force field is reliable. Table 1 indicates the density of the system with different mole fractions of C₆H₆ and its experimental values [30]. It can show in Table 1 that the density of the system gradually increases with the increase of C₆H₆ mole fraction, which is in good agreement with the experimental results [30]. It further shows that the force field selected in the present work is reliable.

3.1.2. Radial Distribution Function and Coordination Numbers

The radial distribution function (RDF) represents the distribution of other atoms in the spherical shell of radius r from the central target atom and thickness δr . It reflects the structural characteristic of a particle in the system, and the coordination numbers of other parti-

cles around the central atom can be obtained by integrating the RDF. In chloroaluminate-type ionic liquids with the mole fraction of AlCl_3 is 0.667 (AlCl_3 : chloroaluminate-type ionic liquids is 2:1), aluminum ion mainly exists in the form of Al_2Cl_7^- . Therefore, for the convenience of discussion, we define it as $\text{Al}_x\text{Cl}_y^{3x-y}$. Figure 2 shows radial distribution function between $[\text{Et}_3\text{NH}]^+$ and $\text{Al}_x\text{Cl}_y^{3x-y}$, $[\text{Et}_3\text{NH}]^+$ and C_6H_6 , $\text{Al}_x\text{Cl}_y^{3x-y}$ and C_6H_6 , and their coordination numbers with different addition of C_6H_6 . As can be seen from Figure 2a, with the increase of the mole fractions of C_6H_6 , the peak position of the first highest peak moves forward, and the peak becomes larger and larger. It can be seen from Figure 2e that the coordination number of $[\text{Et}_3\text{NH}]^+$ and $\text{Al}_x\text{Cl}_y^{3x-y}$ generally shows a slow downward trend. It shows that the addition of benzene weakens the interaction between anions and cations, and benzene occupies the position of original ions, which further reduces the association degree of main ion aggregates in ionic liquids, which confirms the experimental conclusion of Abbott et al. [55].

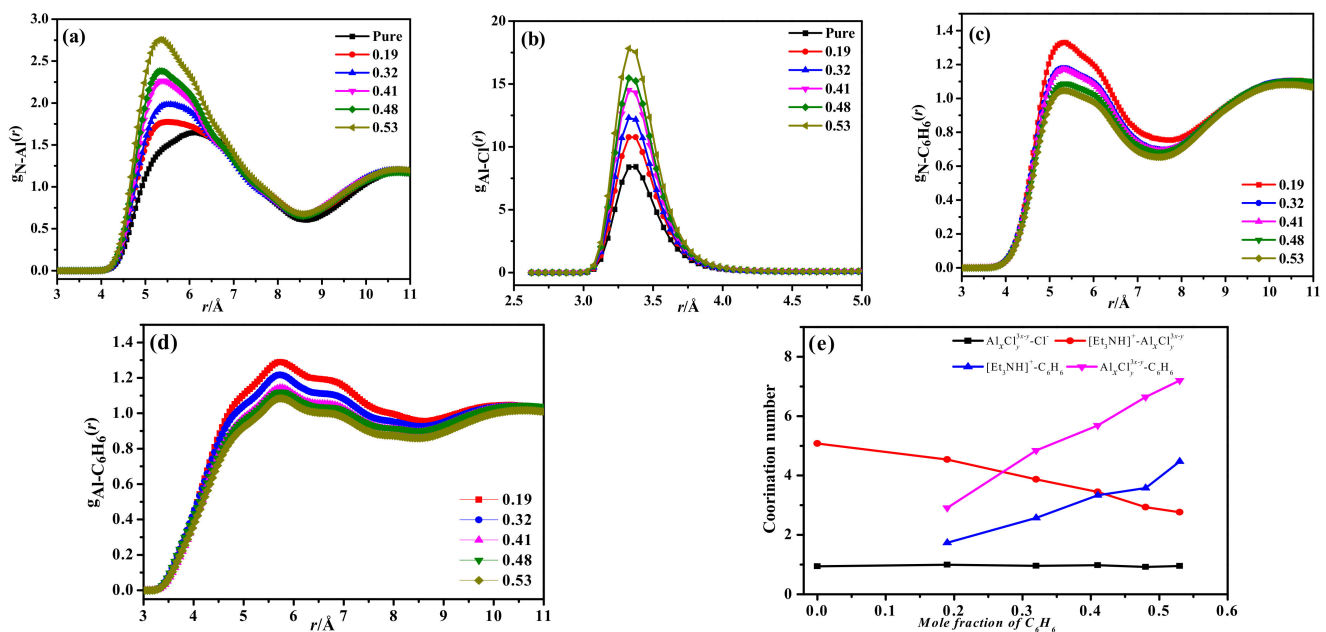


Figure 2. Radial distribution functions and coordination number from molecular dynamics. (a) $[\text{Et}_3\text{NH}]^+ - \text{Al}_x\text{Cl}_y^{3x-y}$, (b) $\text{Al}_x\text{Cl}_y^{3x-y} - \text{Cl}^-$, (c) $[\text{Et}_3\text{NH}]^+ - \text{C}_6\text{H}_6$, (d) $\text{Al}_x\text{Cl}_y^{3x-y} - \text{C}_6\text{H}_6$, and (e) coordination number.

It can be observed in Figure 2b that the peak value of the radial distribution function of $\text{Al}_x\text{Cl}_y^{3x-y}$ and Cl^- is very large, and there is an obvious sharp peak at 3.35 Å. This indicates that an obvious Cl^- polymerization layer is formed around $\text{Al}_x\text{Cl}_y^{3x-y}$. With the increase of C_6H_6 , the peak value of the radial distribution function of $\text{Al}_x\text{Cl}_y^{3x-y}$ and Cl^- is higher and higher, indicating that the interaction between $\text{Al}_x\text{Cl}_y^{3x-y}$ and Cl^- is weaker and weaker. It can be seen from Figure 2e that after the addition of C_6H_6 , the coordination number of $\text{Al}_x\text{Cl}_y^{3x-y}$ and Cl^- is between 0.99 and 0.92, indicating that Al ion mainly exists as Al_2Cl_7^- . As can be seen from Figure 2b,c, with the increase of the mole fractions of C_6H_6 , the peak value of the radial distribution function of $[\text{Et}_3\text{NH}]^+$ and $\text{Al}_x\text{Cl}_y^{3x-y}$ and C_6H_6 in the system gradually decrease. The radial distribution functions of $[\text{Et}_3\text{NH}]^+$ and C_6H_6 had a discernible peak, while the radial distribution functions of $\text{Al}_x\text{Cl}_y^{3x-y}$ and C_6H_6 had no obvious peak, and their peak shoulders are wide. As showed in Figure 2e, with the increase of C_6H_6 mole fraction, the number density of C_6H_6 in the system increases, resulting in an increase in the chance of contact with cations, so that the coordination numbers of $[\text{Et}_3\text{NH}]^+$ with C_6H_6 , $\text{Al}_x\text{Cl}_y^{3x-y}$ and C_6H_6 gradually increase. This further shows that the addition of C_6H_6 weakens the interaction between cation and anion.

3.1.3. Spatial Distribution Function

The spatial distribution function describes the geometric distribution of relevant components in the system in three-dimensional space. According to the simulated data, the spatial distribution function can be made with gopenmol software [53]. Figure 3 displays the three-dimensional spatial distribution of $[\text{Et}_3\text{NH}]^+$ and other ions around aluminum coordination ions when the mole fraction of C_6H_6 is 0.41 (other mole fractions are similar). Figure 3a shows the three-dimensional spatial distribution of C_6H_6 (green), Cl^- (yellow) and $\text{Al}_x\text{Cl}_y^{3x-y}$ (red) around $[\text{Et}_3\text{NH}]^+$. The green area indicates the distribution when the distribution density is 2 times the average density, and the yellow area and red area show the distribution when the distribution density of Cl^- and $\text{Al}_x\text{Cl}_y^{3x-y}$ is 5 times the average density. Figure 3b displays the three-dimensional spatial distribution of Cl^- (yellow) and C_6H_6 (green) around $\text{Al}_x\text{Cl}_y^{3x-y}$. The distribution density of yellow and green areas is 5 times and 2 times of the average density respectively.

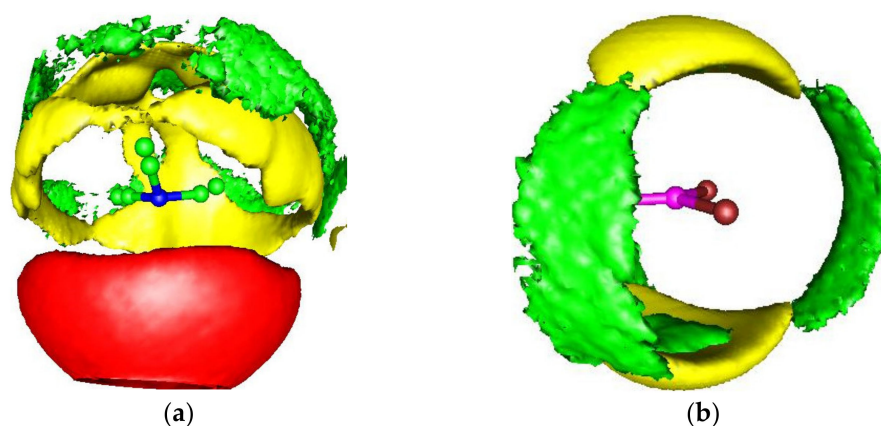


Figure 3. The calculated three-dimensional spatial distributions. (a) Cl^- (yellow), $\text{Al}_x\text{Cl}_y^{3x-y}$ (red), and C_6H_6 (green) around $[\text{Et}_3\text{NH}]^+$; (b) C_6H_6 (green), Cl^- (yellow) around $\text{Al}_x\text{Cl}_y^{3x-y}$.

From Figure 3a, we can find that benzene is mainly distributed on the side of $[\text{Et}_3\text{NH}]^+$ and on the outer layer of chloride anions, but not between $[\text{Et}_3\text{NH}]^+$ and $\text{Al}_x\text{Cl}_y^{3x-y}$. It is consistent with the distribution law of the corresponding radial distribution function in Figure 2a,b. It can be seen from Figure 3b that chloride anions distributed around aluminum atoms is distributed around $\text{Al}_x\text{Cl}_y^{3x-y}$, closer to the upper and lower sides of aluminum atoms, while benzene is distributed around $\text{Al}_x\text{Cl}_y^{3x-y}$ and closer to chlorine atoms.

3.1.4. Self-Diffusion Coefficient

The diffusion coefficients are obtained from Einstein equation [56] as showed in Equation (1), namely,

$$D_i = \frac{1}{6} \lim_{t \rightarrow \infty} \frac{d}{dt} \langle [r_i(t) - r_i(0)]^2 \rangle. \quad (1)$$

where $[r_i(t) - r_i(0)]$ is the mean square displacement (MSD) of i particle. $\langle \cdot \rangle$ is the ensemble average, $r_i(t)$ is the position of particle i at time t .

Figure 4 shows the mean square displacement (MSD) of $[\text{Et}_3\text{NH}]\text{Cl}/\text{AlCl}_3$ with C_6H_6 mole fraction of 0.19 and the effect of C_6H_6 on the diffusion coefficient of each particle in the system. We can see in Figure 4a that the MSD of all ions are linear, which means that the system is a homogeneous solution and attained a self-diffusion state. As shown in Figure 4b, with the increase of C_6H_6 mole fraction, the diffusion coefficients of $[\text{Et}_3\text{NH}]^+$, Al_2Cl_7^- and C_6H_6 in the system continue to increase, and the diffusion coefficient follows $\text{C}_6\text{H}_6 > \text{Al}_x\text{Cl}_y^{3x-y} > [\text{Et}_3\text{NH}]^+$. With the addition of C_6H_6 , the interaction between anions and cations in the system decreases also dilutes the electrolyte, therefore the diffusion ability of anions and cations in the system increases, which will help to improve the electro-

chemical properties of the system, such as reducing viscosity and increasing conductivity, which is consistent with the experimental results.

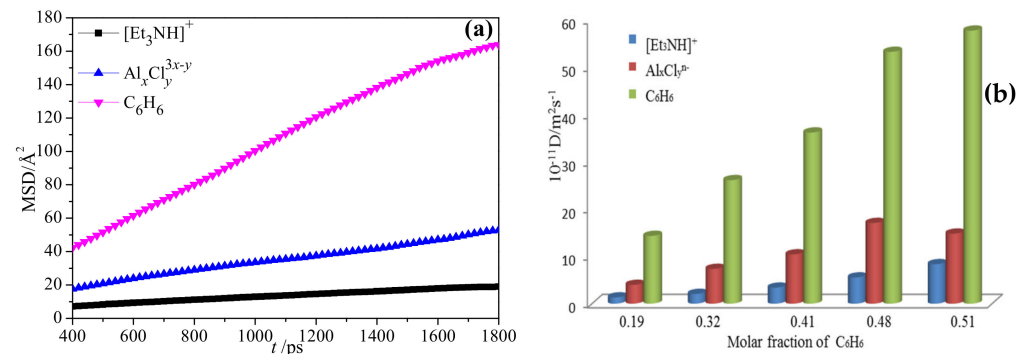


Figure 4. (a) MSD ($x_{\text{AlCl}_3} = 0.19$) and (b) the diffusion coefficient of each ion in [Et₃NH]Cl/AlCl₃ with different mole fraction of C₆H₆ from molecular dynamics simulation.

3.1.5. Viscosity and Conductivity

Viscosity is obtained by Stokes-Einstein relation of Equation (2) [57],

$$\eta_i D_i = \eta_j D_j, \quad (2)$$

where η_i , η_j , D_i , D_j represents the viscosity and self-diffusion coefficient of two liquids at a specific temperature. The viscosity η_j and self-diffusion coefficient D_j of water can be selected as the standard, which are η_j and D_j is 9×10^{-4} Pa·s and 2.30×10^{-9} m²/s [58,59] respectively at 298.15 K.

Conductivity (κ) [60] is obtained from Nernst-Einstein equation in Equation (3),

$$\kappa = \frac{Nq^2}{k_B T} (D_+ + D_-) \quad (3)$$

where N is the number of ions in per unit volume, q is the electron charge, D_+ is the self-diffusion coefficient of cation, D_- is the self-diffusion coefficient of anion, and k_B is the Boltzmann constant (1.38×10^{-23} J/K).

Figure 5 shows the effects of C₆H₆ on the viscosity and conductivity of [Et₃NH]Cl/AlCl₃ ionic liquid system. It can be seen from Figure 5 that with the increase of C₆H₆ mole fraction, the viscosity of the system continues to decrease and the conductivity gradually increases, which is consistent with the change trend of experimental [30]. According to the previous analysis, the addition of C₆H₆ reduces the interaction between anions and cations, and also dilutes the electrolyte, so the viscosity of the system decreases, the ion diffusion in the system accelerates, and the conductivity of the system increases. When $x < 0.4$, the viscosity of the system can be reduced rapidly by adding C₆H₆. When $x > 0.4$, the viscosity of the system changes little by adding C₆H₆, indicating that the system is basically saturated.

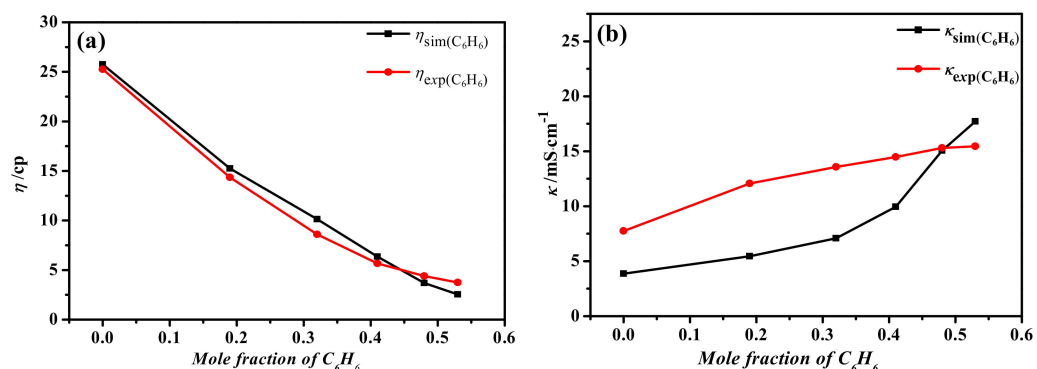


Figure 5. Effects of the C_6H_6 mole fractions on viscosity (a) and conductivity (b) in $[Et_3NH]Cl/AlCl_3$ system.

3.2. Structure, Frontier Orbitals and Adsorption of Cations, Anions and Additives on Surface

According to the above molecular dynamics simulation and experimental results [30], the main aluminum anions mainly exists in the form of $Al_2Cl_7^-$ in $[Et_3NH]Cl/AlCl_3$ ionic liquid system. Therefore, for anions in the system, we only consider $Al_2Cl_7^-$. Figure 6 shows the HOMO and LUMO distribution of $[Et_3NH]^+$, $Al_2Cl_7^-$ and C_6H_6 obtained by B3LYP/6-311++g(d,p) method. It can be seen from Figure 6 that HOMO of $[Et_3NH]^+$ is mainly distributed on the carbon atoms of three ethyl groups connected with N atom, and the LUMO is concentrated on H connected with N atom. The HOMO of $Al_2Cl_7^-$ is mainly distributed on the chlorine atom connected to the aluminum with a single bond. LUMO contributes almost every chlorine atom, while the HOMO and LUMO of benzene are concentrated on the ring. Therefore, $[Et_3NH]^+$, $Al_2Cl_7^-$ and C_6H_6 may be adsorbed on the metal surface in parallel, which agrees well with the results obtained from frontier orbitals.

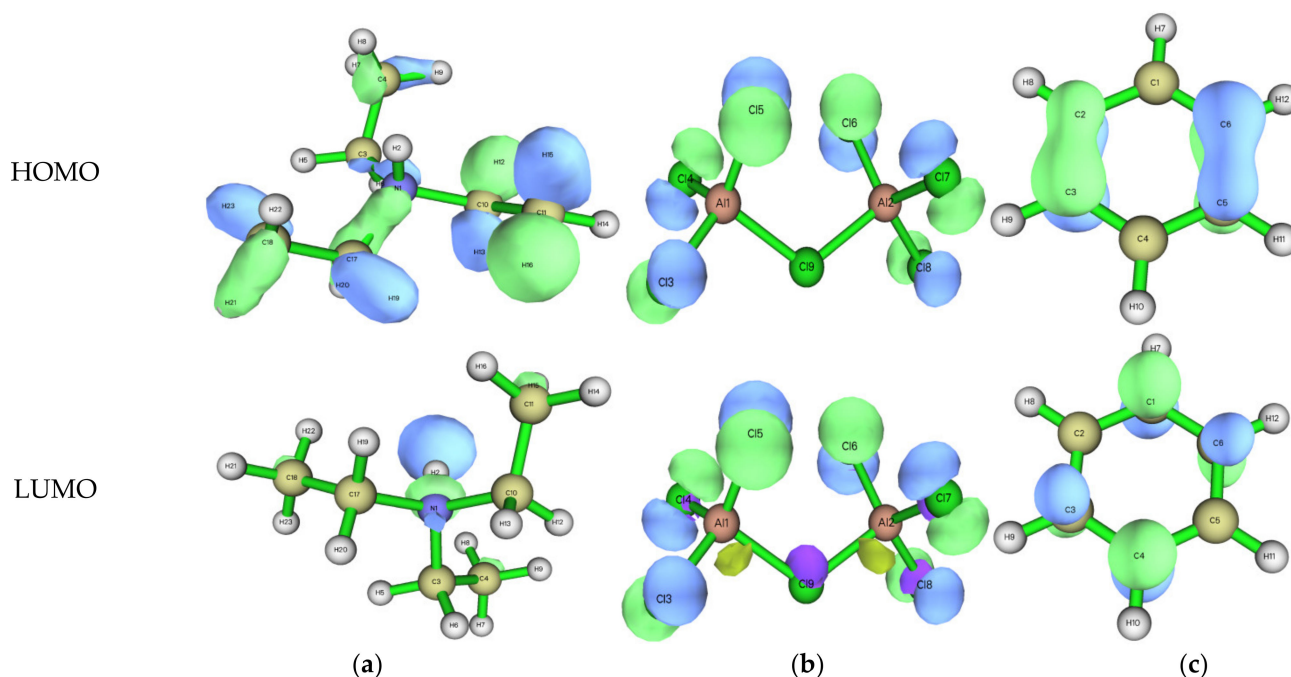


Figure 6. The calculated HOMO and LUMO from B3LYP/6-311++G(d,p) for (a) Et_3NH^+ ; (b) $Al_2Cl_7^-$ and (c) C_6H_6 . The green and blue color in the figure represents the positive phases and negative phases of the orbital respectively.

Figure 7 shows Electrostatic potential distribution diagram of $[Et_3NH]^+$, $Al_2Cl_7^-$ and C_6H_6 obtained by B3LYP/6-311++G(d,p) method. From the Figure 7, it can be seen that the whole positive electrostatic potential surface of $[Et_3NH]^+$ is distributed in the outer

layer; the maximum electrostatic potential comes from the H atom(H0) bonded with central N atom and the region between the hydrogen atom (H1, H3 and H5) in the methyl on the ethyl chain and the hydrogen atom (H2, H4 and H6) in the methylene on the other ethyl chain, such as the zone between the H1 and H6, the zone between H2 and H3, as well as the zone of H4 and H5. The electrostatic potential in these regions is greater than 100 kcal/mol. The negative electrostatic potential is distributed outside of Al_2Cl_7^- , which is mainly distributed on Cl atoms. For benzene molecule, the positive electrostatic potential is distributed in the outer layer, while the negative electrostatic potential is distributed in the inner layer, mainly distributed around C atoms.

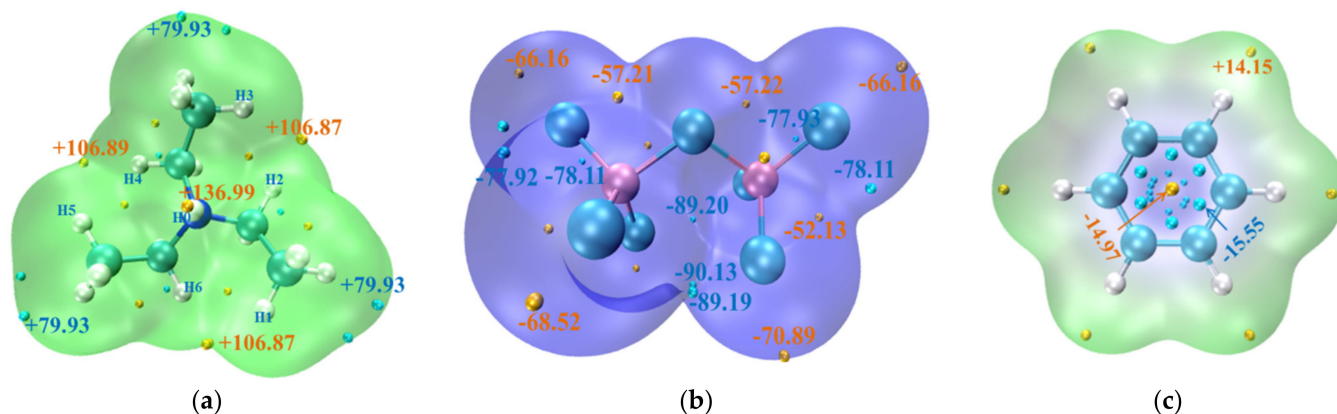


Figure 7. Electrostatic potential mapped molecular vdW surface of calculated by B3LYP/6-311++G(d,p) for (a) Et_3NH^+ ; (b) Al_2Cl_7^- and (c) C_6H_6 . Green and blue represent positive and negative electrostatic potential distribution respectively. The yellow and green points represent the maximum and minimum values of electrostatic potential respectively.

Figure 8 gives the optimized adsorption configuration of $[\text{Et}_3\text{NH}]^+$, Al_2Cl_7^- and C_6H_6 adsorbed on Cu(111) surface. It can be observed from Figure 8a that $[\text{Et}_3\text{NH}]^+$ is adsorbed on the Cu(111) surface in parallel, which is consistent with the results of frontier orbital and electrostatic potential analysis. The nearest distances between H atom bonded to N of $[\text{Et}_3\text{NH}]^+$ and Cu atoms on the surface are 2.548 Å for H3-Cu3, 2.596 Å for H4-Cu4, 2.621 Å for H1-Cu1, 2.620 Å for H2-Cu2, respectively. It can be seen that the three nearest lengths between Cu and H are greater than the sum of their covalent radii of 2.07 Å, and close to the sum of its van der Waals radii of 2.8 Å, where the covalent atomic radius of Cu and H is 1.28 Å and 0.79 Å and the van der Waals radius is 1.4 Å and 1.2 Å. Therefore, it suggests that the adsorption process of $[\text{Et}_3\text{NH}]^+$ on Cu (111) surface is a physical adsorption.

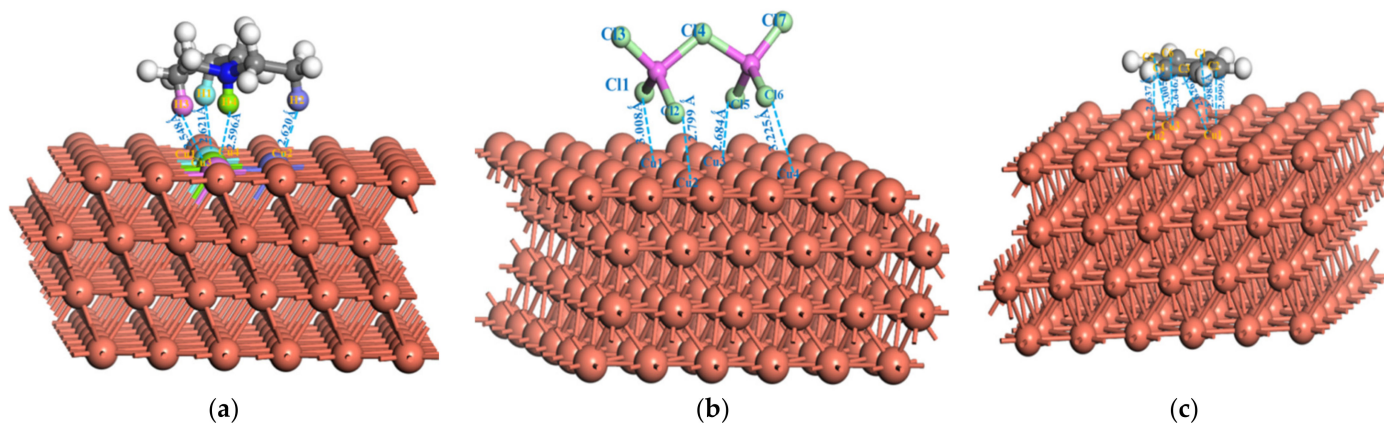


Figure 8. Optimized adsorption configurations of ions adsorbed on Cu(111) surface for (a) Et_3NH^+ ; (b) Al_2Cl_7^- and (c) C_6H_6 .

As showed in Figure 8b, Al_2Cl_7^- lies flat on the Cu(111) surface in the form of four Cl atoms in contact with the Cu atoms of Cu(111) surface. In Figure 8b, we found that the minimum distances between Cl atom of Al_2Cl_7^- and Cu atoms of surface are 2.684 Å for Cu3-Cl5, 2.799 Å for Cu2-Cl2 and 3.008 Å for Cu1-Cl1, and 3.225 Å for Cu4-Cl6, respectively. However, the three minimum distances between Cu and Cl are greater than the sum of their atomic radii of 2.27 Å, and close to the sum of its van der Waals radius of 3.15 Å, where the covalent atomic radius of Cu and Cl are 1.28 Å and 0.99 Å, and the van der Waals radius are 1.4 Å and 1.75 Å, respectively. It means that the adsorption of Al_2Cl_7^- on Cu(111) surface is also a physical adsorption process.

It can be observed in Figure 8c that the benzene ring plane is adsorbed on the Cu(111) surface in parallel, which is consistent with the results of frontier orbital and electrostatic potential analysis. The nearest distance between the six C atoms in the benzene ring and the Cu atoms on the Cu(111) is 2.626 Å for Cu1-C2, 2.637 Å for Cu2-C4, 2.646 Å for Cu3-C6, 2.988 Å for Cu1-C1, 2.999 Å for Cu1-C3 and 3.005 Å for Cu3-C5, respectively. The distances of the six nearest Cu and C are located at the sum of the covalent atomic radii of Cu and C of 2.05 Å and the sum of its van der Waals radius 3.1 Å, where the atomic radii of Cu and C are known to be 1.28 and 0.77 Å, and the van der Waals radii are 1.4 Å and 1.70 Å, respectively. Therefore, the adsorption of benzene on Cu surface is a physical adsorption process, which is consistent with other research results. [27,28]

It can be seen from Table 2 that the order of adsorption energy of $[\text{Et}_3\text{NH}]^+$, Al_2Cl_7^- and C_6H_6 on the Cu(111) surface is $[\text{Et}_3\text{NH}]^+ > \text{C}_6\text{H}_6 > \text{Al}_2\text{Cl}_7^-$. Combined with the structural analysis of adsorption and the results of molecular dynamics simulation, the diffusion of benzene is fastest in $[\text{Et}_3\text{NH}]\text{Cl}/\text{AlCl}_3$ ionic liquid system, and benzene is easier to be adsorbed to the cathode electrode surface than Al_2Cl_7^- anion in the electrolysis process, so as to reduce the effective surface area of the cathode and slow down the reduction speed of Al_2Cl_7^- ion on the cathode surface. At the same time, the protruding part tiled on the electrode surface plays a certain leveling role. Therefore, a bright metal deposition layer can be obtained in the deposition process [55–58].

Table 2. The adsorption energy total charge transfer (Δq) of $[\text{Et}_3\text{NH}]^+$, Al_2Cl_7^- and C_6H_6 on Cu(111).

Adsorption	$E_{\text{Cu(111)}} \text{ (eV)}$	$E_{\text{mol}} \text{ (eV)}$	$E_{\text{Cu(111)-Mol}} \text{ (eV)}$	$E_{\text{ads}} \text{ (kJ.mol}^{-1}\text{)}$	$\Delta q \text{ (e)}$
Cu(111)/ $[\text{Et}_3\text{NH}]^+$	−567.2566	−117.3809	−689.5731	−476.2151	0.277
Cu(111)/ C_6H_6	−567.2566	−76.3256	−644.6412	−102.1741	−0.045
Cu(111)/ Al_2Cl_7^-	−567.2566	−38.7584	−604.0223	192.2199	−0.172

Figure 9 shows the calculated differential charge density of $[\text{Et}_3\text{NH}]^+$, Al_2Cl_7^- and C_6H_6 adsorbed on Cu(111) surface. Charge accumulated is negative in Figure 9. The yellow part represents the area of charge accumulation, and blue part represents the area of charge reduction. It can be seen from Figure 9a that the four hydrogen atoms and the whole region of the cation $[\text{Et}_3\text{NH}]^+$ near Cu(111) surfaces are yellow, indicating that it is the area of charge accumulation, while the blue area around the lower copper atom indicates that the surface charge of Cu (111) is reduced. The three ethyl chains are blue regions, indicating that their charge decreases after adsorption, which is consistent with the fact that the alkyl chain is an electron donor group. The changes of Bader charges after adsorption are shown in the last column in Table 2. It can be seen from Table 2 that Cu(111) transfer a charge of 0.277 e to $[\text{Et}_3\text{NH}]^+$. The results demonstrate that the interaction between $[\text{Et}_3\text{NH}]^+$ and Cu(111) is strong, which is consistent with the results of adsorption energy.

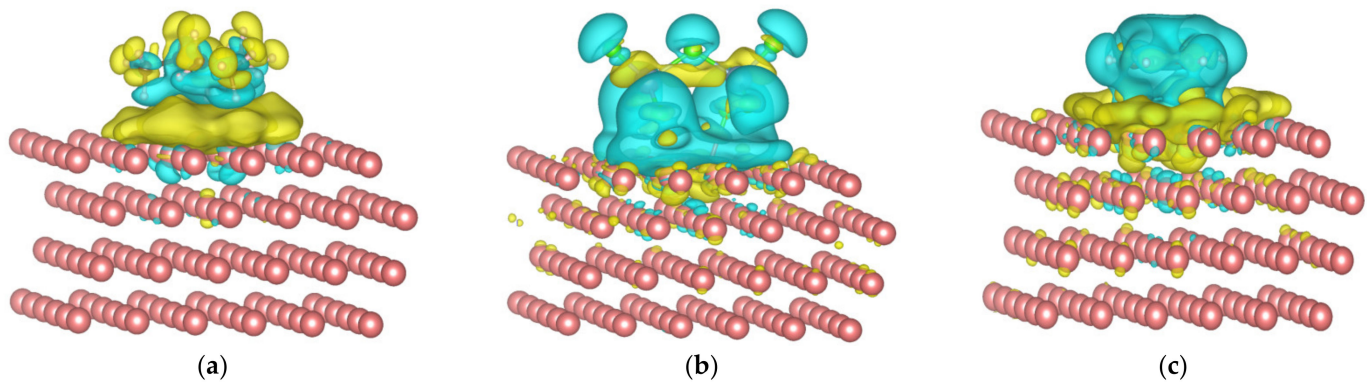


Figure 9. Differential charge density diagram of molecules or ions on the surface of Cu(111) for (a) Et_3NH^+ ; (b) Al_2Cl_7^- and (c) C_6H_6 . The yellow color represents the area of charge accumulation and blue color represents the area of charge reduction.

It can be seen from Figure 9b that three chlorine atoms near Cu(111) surface on Al_2Cl_7^- are blue, indicating that the charge in this area is reduced. Some atoms on Cu(111) in the region below Al_2Cl_7^- are yellow, indicating that the charge in these areas increases. It can be seen from Table 2 that Al_2Cl_7^- transfers a charge of 0.172 e to Cu(111) surface. As can be observed in Figure 9c, the ring of benzene is adsorbed on Cu(111) surface in the form of π - π stacking. The carbon atoms on the benzene ring are blue, indicating that the charge in this area is reduced, and the carbon atoms in the first and second layers of Cu(111) are yellow, indicating that the charges in these areas are increased. It can be seen from Table 2 that benzene transfers a charge of 0.045e to Cu(111).

As discussed above, the addition of benzene into the $[\text{Et}_3\text{NH}]\text{Cl}/\text{AlCl}_3$ ionic liquid system reduces interaction between the cation and the anion. It decreases the viscosity of the system and improves the diffusion ability of cation and anion in the system. Therefore, it enhances the conductivity and improves the electrochemical properties of the system. The results of first principle calculation show that the adsorption energy between benzene and metal is stronger than that of aluminum ion, so benzene would be easier to adsorb on the electrode surface, so as to reduce the effective surface area of the cathode, slow down the reduction speed of Al_2Cl_7^- on the cathode surface and increase the over-potential, which is consistent with the experimental CV curve results [30]. At the same time, benzene is tiled on the protruding part of the electrode surface to play a certain leveling role. Therefore, for the electrodeposition of aluminum in ionic liquids, the addition of benzene is conducive to the refinement of sediment grains. This is consistent with the research results that benzene can be used as an additive in most ionic liquid electrodeposited aluminum to obtain grain-refined deposition layers [29,61,62].

4. Conclusions

The effect of benzene on the radial distribution function, coordination number, spatial distribution function, physical and chemical properties such as density, viscosity, conductivity and transport properties of $[\text{Et}_3\text{NH}]\text{Cl}/\text{AlCl}_3$ ionic liquid were studied by the combination of first principle calculation and molecular dynamics simulation. It was found that the density of the system decreases gradually with the addition of benzene. Benzene is situated near to the cation $[\text{Et}_3\text{NH}]^+$ of ionic liquid, which weakens the interaction between cation and anion, reduces the viscosity of the system, increases the diffusion of ions and increases the conductivity. Aluminum coordination is in the form of Al_2Cl_7^- in the present system. The order of the diffusion coefficient is $\text{C}_6\text{H}_6 > \text{Al}_x\text{Cl}_y^{3x-y} > [\text{Et}_3\text{NH}]^+$. The simulated density, viscosity and conductivity agree well with the experimental values. The order of the adsorption energy of ions on metal is $[\text{Et}_3\text{NH}]^+ > \text{C}_6\text{H}_6 > \text{Al}_2\text{Cl}_7^-$, indicating that benzene is more easily adsorbed on the electrode surface than the electroactive ions Al_2Cl_7^- . Therefore, benzene would be easier to adsorb on the electrode surface, so as to decrease the effective surface area of the cathode, slow down the reduction speed of Al_2Cl_7^- on the cathode surface and increase the over-potential. At the same time, benzene

is absorbed on the protruding part of the electrode surface to play a certain leveling role, so the grain refined deposition layers can be obtained in electrodeposition.

Author Contributions: Conceptualization, methodology, investigation, and writing of the original draft preparation were done by G.T., whereas the partial computational work of absorption was done by H.D. and Q.Y. All authors have read and agreed to the published version of the manuscript.

Funding: This research was funded by National Natural Science Foundation of China (grant numbers 51774158, 5126402) and Cultivating Plan Program for the Leader in Science and Technology of Yunnan Province (grant number 2011HR013).

Institutional Review Board Statement: Not applicable.

Informed Consent Statement: Not applicable.

Data Availability Statement: Data is contained within the article.

Acknowledgments: The authors wish to thank the National Natural Science Foundation of China and the Department of Science and Technology of Yunnan Province for their support on the project no. 51774158, 51264021, and the project no. 2011HR013.

Conflicts of Interest: The authors declare no conflict of interest. The funders had no role in the design of the study; in the collection, analyses, or interpretation of data; in the writing of the manuscript, or in the decision to publish the results.

References

1. Zhang, S.J.; Lu, X.M. *Ionic Liquids, from Basic Research to Industrial Application*; Science Press: Beijing, China, 2006.
2. Deng, Y.Q. *Ionic Liquids-Properties, Preparation and Application*; China Petrochemical Press: Beijing, China, 2006.
3. Abbott, A.P.; McKenzie, K.J. Application of ionic liquids to the electrodeposition of metals. *Phys. Chem. Chem. Phys.* **2006**, *8*, 4265–4279. [[CrossRef](#)] [[PubMed](#)]
4. Tian, G.C.; Li, J.; Hua, Y.X. Application of ionic liquids in metallurgy of nonferrous metals. *Chin. J. Process. Eng.* **2009**, *9*, 200.
5. Tian, G.C.; Li, J.; Hua, Y.X. Application of ionic liquids in hydrometallurgy of nonferrous metals. *Trans. Nonferrous Met. Soc.* **2010**, *20*, 513–520. [[CrossRef](#)]
6. Zhang, M.; Kamavarum, V.; Reddy, R.G. New electrolytes for aluminum production: Ionic liquids. *JOM* **2003**, *55*, 54–57. [[CrossRef](#)]
7. Liu, F.; Deng, Y.; Han, X. Electrodeposition of metals and alloys from ionic liquids. *J. Alloy. Compd.* **2016**, *654*, 163–170. [[CrossRef](#)]
8. Zhong, X.W.; Xiong, T.; Lu, J.; Shi, Z.N. Advances of electro-deposition and aluminum refining of aluminum and aluminum alloy ionic liquid electrolyte system. *Nonferrous Met. Sci. Eng.* **2014**, *5*, 44.
9. Liu, Y.X.; Li, J. *Modern Aluminum Electrolysis*; Metallurgical Industry Press: Beijing, China, 2008.
10. Carlin, R.T.; Crawford, W.; Bersch, M. Nucleation and morphology studies of aluminum deposited from an ambient-temperature chloroaluminate molten salt. *J. Electrochem. Soc.* **1992**, *139*, 2720–2727. [[CrossRef](#)]
11. Suneesh, P.V.; Babu, T.S.; Ramachandran, T. Electrodeposition of aluminium and aluminium-copper alloys from a room temperature ionic liquid electrolyte containing aluminium chloride and triethylamine hydrochloride. *Int. J. Miner. Metall. Mater.* **2013**, *20*, 909–916. [[CrossRef](#)]
12. Xu, H.; Bai, T.; Chen, H. Low-cost $\text{AlCl}_3/\text{Et}_3\text{NHCl}$ electrolyte for high-performance aluminum-ion battery. *Energy Storage Mater.* **2019**, *17*, 38–45. [[CrossRef](#)]
13. Tian, G.C. Ionic liquids as green electrolytes for Aluminum and Aluminum-alloy production. *Mater. Res. Found.* **2019**, *54*, 249.
14. Ueda, M.; Hariyama, S.; Ohtsuka, T. Al electroplating on the AZ121 Mg alloy in an EMIC- AlCl_3 ionic liquid containing ethylene glycol. *J. Solid State Electrochem.* **2012**, *16*, 3423. [[CrossRef](#)]
15. Liu, L.; Lu, X.; Cai, Y.; Zheng, Y.; Zhang, S. Influence of additives on the speciation, morphology, and nanocrystallinity of aluminum electrodeposition. *Aust. J. Chem.* **2012**, *65*, 1523. [[CrossRef](#)]
16. Zhang, Q.; Wang, Q.; Zhang, S.; Lu, X. Effect of nicotinamide on electrodeposition of Al from aluminum chloride (AlCl_3)-1-butyl-3-methylimidazolium chloride ([BMIM]Cl) ionic liquids. *J. Solid State Electrochem.* **2014**, *18*, 257. [[CrossRef](#)]
17. Wang, Q.; Chen, B.; Zhang, Q.; Lu, X.; Zhang, S. Aluminum deposition from lewis acidic 1-butyl-3-methylimidazolium chloroaluminate ionic liquid ([BMIM]Cl/ AlCl_3) modified with methyl nicotinate. *ChemElectroChem* **2015**, *2*, 1794. [[CrossRef](#)]
18. Wang, Q.; Zhang, Q.; Chen, B.; Lu, X.; Zhang, S. Electrodeposition of bright Al coatings from 1-butyl-3-methylimidazolium chloroaluminate ionic liquids with specific additives. *J. Electrochem. Soc.* **2015**, *162*, D320. [[CrossRef](#)]
19. Sheng, P.F.; Chen, B.; Shao, H.B.; Wang, J.M.; Zhang, J.Q.; Cao, C.N. Electrodeposition and corrosion behavior of nanocrystalline aluminum from a chloroaluminate ionic liquid. *Mater. Corros.* **2015**, *66*, 1338. [[CrossRef](#)]
20. Lang, H.; Zhang, J.; Kang, Y.; Chen, S.; Zhang, S. Effects of lithium bis (oxalato) borate on electrochemical stability of [EMIM][Al_2Cl_7] ionic liquid for aluminum electrolysis. *Ionics* **2017**, *23*, 959. [[CrossRef](#)]

21. Jiang, T.; Brym, M.J.C.; Dubé, G. Electrodeposition of aluminium from ionic liquids: Part II—studies on the electrodeposition of aluminum from aluminum chloride (AlCl₃)-trimethylphenylammonium chloride (TMPAC) ionic liquids. *Surf. Coat. Technol.* **2006**, *201*, 10. [[CrossRef](#)]
22. Jiang, T.; Brym, M.J.C.; Dubé, G. Electrodeposition of aluminium from ionic liquids: Part I—Electrodeposition and surface morphology of aluminium from aluminium chloride (AlCl₃)-1-ethyl-3-methylimidazolium chloride ([EMIm]Cl) ionic liquids. *Surface and Coatings Technology. Surf. Coat. Technol.* **2006**, *201*, 1–9. [[CrossRef](#)]
23. Hou, Y.Y.; Li, R.Q.; Liang, J.; Su, P.B.; Ju, P.F. Electropolishing of Al and Al alloys in AlCl₃/trimethylamine hydrochloride ionic liquid. *Surf. Coat. Technol.* **2018**, *335*, 7. [[CrossRef](#)]
24. Liu, K.R.; Liu, Q.; Han, Q.; Tu, G.F. Electrodeposition of Al on AZ31 magnesium alloy in TMPAC-AlCl₃ ionic liquids. *Trans. Nonferrous Met. Soc.* **2011**, *21*, 2104–2110. [[CrossRef](#)]
25. Su, C.J.; Hsieh, Y.T.; Chen, C.C.; Sun, I.W. Electrodeposition of aluminum wires from the lewis acidic AlCl₃/trimethylamine hydrochloride ionic liquid without using a template. *Electrochem. Commun.* **2013**, *34*, 170–173. [[CrossRef](#)]
26. Bakkar, A.; Neubert, V. Electrodeposition and corrosion characterisation of micro and nano-crystalline aluminium from AlCl₃/1-ethyl-3-methylimidazolium chloride ionic liquid. *Electrochim. Acta* **2013**, *103*, 211–216. [[CrossRef](#)]
27. Gao, L.X.; Wang, L.N.; Qi, T. Electrodeposition of aluminium from AlCl₃/Et₃NHCl ionic liquids. *Acta Phys.-Chim. Sin.* **2008**, *24*, 939–944. [[CrossRef](#)]
28. Liao, Q.; Pitner, W.R.; Stewart, G.; Hussey, C.L.; Stafford, G.R. Electrodeposition of aluminum from the aluminum chloride-1-methyl-3-ethylimidazolium chloride room temperature molten salt + benzene. *J. Electrochem. Soc.* **1997**, *144*, 936–943. [[CrossRef](#)]
29. Uehara, K.; Yamazaki, K.; Gunji, T.; Kaneko, S.; Tanabe, T.; Ohsakab, T.; Matsumoto, F. Evaluation of key factors for preparing high brightness surfaces of aluminum films electrodeposited from AlCl₃-1-ethyl-3-methylimidazolium chloride-organic additive baths. *Electrochim. Acta* **2016**, *215*, 556–565. [[CrossRef](#)]
30. Xia, S.; Zhang, X.M.; Huang, K. Ionic liquid electrolytes for aluminum secondary battery: Influence of organic solvents. *J. Electroanal. Chem.* **2015**, *757*, 167–175. [[CrossRef](#)]
31. Smith, B.; Akimov, A.V. Modeling nonadiabatic dynamics in condensed matter materials: Some recent advances and applications. *J. Phys. Cond. Matter* **2019**, *32*, 073001. [[CrossRef](#)]
32. Tian, G.C.; Wang, D.; Wang, P.F. Molecular Dynamics Simulations of Structure and Properties of 1-Ethyl-3-methylimidazolium Tetrafluoroborate Ionic Liquid and Ethanol Mixtures. *J. Kunming Univ. Sci. Technol.* **2013**, *37*, 21–27.
33. Li, Z.T.; Tian, G.C. Simulation study of the effect of benzene on the structure and properties of 1-ethyl-3-methylimidazolium chloroaluminate. *Comput. Appl. Chem.* **2015**, *32*, 1044.
34. Izgorodina, E.I.; Seeger, Z.L.; Scarborough, D.L.A.; Tan, S.Y.S. Quantum chemical methods for the prediction of energetic, physical, and spectroscopic properties of ionic liquids. *Chem. Rev.* **2017**, *117*, 6696–6754. [[CrossRef](#)] [[PubMed](#)]
35. Wang, X.; Fu, F.; Peng, K. Understanding of structures, dynamics, and hydrogen bonds of imidazolium-based ionic liquid mixture from molecular dynamics simulation. *Chem. Phys.* **2019**, *525*, 110391. [[CrossRef](#)]
36. Varela, L.M.; Méndez-Morales, T.; Carrete, J.; González, B.G.V.; Álvarez, B.D.; Gallego, L.J.; Cabeza, O.; Russinad, O. Solvation of molecular cosolvents and inorganic salts in ionic liquids: A review of molecular dynamics simulations. *J. Mol. Liq.* **2015**, *210*, 178–188. [[CrossRef](#)]
37. Frisch, M.J.E.A.; Trucks, G.W.; Schlegel, H.B.; Scuseria, G.E.; Robb, M.A.; Cheeseman, J.R.; Scalmani, G.; Barone, V.; Mennucci, B.; Petersson, G.; et al. *Gaussian 09 Revision A*, 3rd ed.; Gaussian, Inc.: Wallingford, UK, 2009.
38. Lyubartsev, A.P.; Laaksonen, A.M. DynaMix—a scalable portable parallel MD simulation package for arbitrary molecular mixtures. *Comput. Phys. Commun.* **2000**, *128*, 565–589. [[CrossRef](#)]
39. Wang, J.; Wolf, R.M.; Caldwell, J.W. Development and testing of a general amber force field. *J. Comp. Chem.* **2004**, *25*, 1157–1174. [[CrossRef](#)] [[PubMed](#)]
40. Kim, J.H.; Lee, S.H. Molecular dynamics simulation studies of benzene, toluene, and p-xylene in a canonical ensemble. *Bull. Korean Chem. Soc.* **2002**, *23*, 441–446.
41. De Andrade, J.; Böes, E.S.; Stassen, H. Computational study of room temperature molten salts composed by 1-alkyl-3-methylimidazolium cations force-field proposal and validation. *J. Phys. Chem. B* **2002**, *106*, 13344–13351. [[CrossRef](#)]
42. Wang, J.; Cieplak, P.; Kollman, P.A. How well does a restrained electrostatic potential (RESP) model perform in calculating conformational energies of organic and biological molecules. *J. Comput. Chem.* **2000**, *21*, 1049–1074. [[CrossRef](#)]
43. Kresse, G.; Furthmüller, J. Efficiency of ab-initio total energy calculations for metals and semiconductors using a plane-wave basis set. *Comput. Mater. Sci.* **1996**, *6*, 15–50. [[CrossRef](#)]
44. Kresse, G.; Hafner, J. Ab initio molecular dynamics for liquid metals. *Phys. Rev. B* **1993**, *47*, 558–561. [[CrossRef](#)]
45. Perdew, J.P.; Burke, K.; Ernzerhof, M. Generalized gradient approximation made simple. *Phys. Rev. Lett.* **1996**, *77*, 3865–3868. [[CrossRef](#)]
46. Grimme, S.; Ehrlich, S.; Goerigk, L. Effect of the damping function in dispersion corrected density functional theory. *J. Comput. Chem.* **2011**, *32*, 1456–1503. [[CrossRef](#)] [[PubMed](#)]
47. Padama, A.A.; Kishi, H.; Arevalo, R.L.; Moreno, J.L.V.; Kasai, H.; Taniguchi, M.; Uenishi, M.; Tanaka, H.; Nishihata, Y. NO dissociation on Cu(111) and Cu₂O(111) surfaces: A density functional theory based study. *J. Phys. Condens. Matter* **2012**, *24*, 175005. [[CrossRef](#)]
48. Lide, D.R. *CRC Handbook of Chemistry and Physics*, 84th ed.; CRC Press: Los Angeles, CA, USA, 2003–2004.

49. Silbaugh, T.L.; Giorgi, J.B.; Xu, Y.; Tillekaratne, A.; Zaera, F.; Campbell, C.T. Adsorption energy of tert-Butyl on Pt (111) by dissociation of tert-Butyl Iodide: Calorimetry and DFT. *J. Phys. Chem. C* **2014**, *118*, 427–438. [[CrossRef](#)]
50. Methfessel, M.; Paxton, A.T. High-precision sampling for Brillouin-zone integration in metals. *Phys. Rev. B Condens. Matter* **1989**, *40*, 3616–3621. [[CrossRef](#)] [[PubMed](#)]
51. Bader, R.F.W. *Atoms in Molecules: A Quantum Theory*; Oxford University Press: Oxford, UK, 1990.
52. Momma, K.; Izumi, F. VESTA 3 for three-dimensional visualization of crystal, volumetric and morphology data. *J. Appl. Crystallogr.* **2011**, *44*, 1272–1276. [[CrossRef](#)]
53. Lu, T.; Chen, F. Multiwfn: A multifunctional wavefunction analyzer. *J. Comput. Chem.* **2012**, *33*, 580–592. [[CrossRef](#)] [[PubMed](#)]
54. Laaksonen, L. A graphics program for the analysis and display of molecular dynamics trajectories. *J. Mol. Graph.* **1992**, *10*, 33–34. [[CrossRef](#)]
55. Abbott, A.P.; Qiu, F.; Abood, H.M.; Ali, M.R.; Ryder, K.S. Double layer, diluent and anode effects upon the electrodeposition of aluminum from chloroaluminate based ionic liquids. *Phys. Chem. Chem. Phys.* **2010**, *12*, 1862. [[CrossRef](#)] [[PubMed](#)]
56. Liu, J.; Cao, D.; Zhang, L. Molecular dynamics study on nanoparticle diffusion in polymer melts: A test of the Stokes-Einstein law. *J. Phys. Chem. C* **2008**, *112*, 6653–6661. [[CrossRef](#)]
57. Morrow, T.I.; Maginn, E.J. Molecular dynamics study of the ionic liquid 1-n-butyl-3-methylimidazolium hexafluorophosphate. *J. Phys. Chem. B* **2002**, *106*, 12807–12813. [[CrossRef](#)]
58. Banipal, P.K.; Chahal, A.K.; Singh, V.; Banipal, T.S. Rheological behaviour of some saccharides in aqueous potassium chloride solutions over temperature range (288.15 to 318.15) K. *J. Chem. Thermodynam.* **2010**, *42*, 1024–1035. [[CrossRef](#)]
59. Holz, M.; Heil, S.R.; Sacco, A. Temperature-dependent self-diffusion coefficients of water and six selected molecular liquids for calibration in accurate ¹H NMR PFG measurements. *Phys. Chem. Chem. Phys.* **2000**, *2*, 4740–4742. [[CrossRef](#)]
60. Noda, A.; Hayamizu, K.; Watanabe, M. Pulsed-gradient spin-echo ¹H and ¹⁹F NMR ionic diffusion coefficient, viscosity, and ionic conductivity of non-chloroaluminate room-temperature ionic liquids. *J. Phys. Chem. B* **2001**, *105*, 4603–4610. [[CrossRef](#)]
61. Fang, Y.; Yoshii, K.; Jiang, X.; Sun, X.; Tsuda, T.; Mehio, N.; Dai, S. An AlCl₃ based ionic liquid with a neutral substituted pyridine ligand for electrochemical deposition of aluminum. *Electrochim. Acta* **2015**, *160*, 82–88. [[CrossRef](#)]
62. Pulletikurthi, G.; Bödecker, B.; Borodin, A.; Weidenfeller, B.; Endres, F. Electrodeposition of Al from a 1-butylpyrrolidine-AlCl₃ ionic liquid. *Prog. Nat. Sci. Mater. Int.* **2015**, *25*, 603–611. [[CrossRef](#)]